Articles

Structure and Function of Residue 104 and Water Molecules in the Xenobiotic Substrate-Binding Site in Human Glutathione *S*-Transferase P1-1[†,‡]

Xinhua Ji,*[,§] Jaroslaw Blaszczyk,[§] Bing Xiao,[§] Rosemary O'Donnell,[§] Xun Hu,[∥] Christian Herzog,[⊥] Shivendra V. Singh,[∥] and Piotr Zimniak[⊥]

ABL-Basic Research Program, National Cancer Institute−Frederick Cancer Research and Development Center, Frederick, Maryland 21702, Departments of Medicine and of Biochemistry & Molecular Biology, University of Arkansas for Medical Sciences, and VA John McClellan Memorial Hospital, Little Rock, Arkansas 72205, and Cancer Research Laboratory, Mercy Hospital of Pittsburgh, Pittsburgh, Pennsylvania 15219

Received March 23, 1999; Revised Manuscript Received June 8, 1999

ABSTRACT: Two variants of human class π glutathione (GSH) *S*-transferase 1-1 with either isoleucine or valine in position 104 (hGSTP1-1[I104] and hGSTP1-1[V104]) have distinct activity toward (+)-*anti*-7,8-dihydroxy-9,10-oxy-7,8,9,10-tetrahydrobenzo[*a*]pyrene [(+)-*anti*-BPDE]. To elucidate their structure−function relationship, we determined the crystal structures of the two variants in complex with GSBpd, the GSH conjugate of (+)-*anti*-BPDE, at 2.1 and 2.0 Å resolution, respectively. The crystal structures reveal that residue 104 in the xenobiotic substrate-binding site (H-site) dictates the binding modes of the product molecule GSBpd with the following three consequences. First, the distance between the hydroxyl group of Y7 and the sulfur atom of GSBpd is 5.9 Å in the hGSTP1-1[I104]·GSBpd complex versus 3.2 Å in the V104 variant. Second, one of the hydroxyl groups of GSBpd forms a direct hydrogen bond with R13 in hGSTP1-1[V104]·GSBpd; in contrast, this hydrogen bond is not observed in the I104 complex. Third, in the hydrophilic portion of the H-site of the I104 complex, five H-site water molecules [Ji, X., et al. (1997) *Biochemistry 36*, 9690−9702] are observed, whereas in the V104 complex, two of the five have been displaced by the Bpd moiety of GSBpd. Although there is no direct hydrogen bond between Y108 (OH) and the hydroxyl groups of GSBpd, indirect hydrogen bonds mediated by water molecules are observed in both complexes, supporting the previously suggested role of the hydroxyl group of Y108 as an electrophilic participant in the addition of GSH to epoxides.

Glutathione *S*-transferases (GSTs, EC 2.5.1.18)[1] catalyze the addition of the tripeptide glutathione (GSH) to xenobiotic substrates that have electrophilic functional groups. The catalytic diversity of this family of detoxification enzymes arises, in part, from the existence of at least seven distinct gene classes: α, μ, π, σ, θ, κ, and microsomal GSTs. Although each isozyme generally exhibits a relatively broad substrate selectivity, most have unique catalytic attributes that are important in defining the ability of the isozyme to metabolize a particular set of endogenous and xenobiotic electrophiles (*1*−*3*). The extent of understanding the precise enzyme−substrate interactions responsible for the catalytic properties has been greatly increased by the recent determinations of many three-dimensional structures of GSTs. Both the GSH-binding site (G-site) and the xenobiotic substrate-binding site (H-site) can be seen in these crystal structures. The G-site is very well defined for cytosolic GSTs for which three-dimensional structures are available. Three different GSH-binding modes have been observed, as summarized by Ji et al. (*4*). In contrast, the binding modes of xenobiotic substrates and product molecules are much more complex and class specific. For example, the H-site in rGSTM1-1 is a hydrophobic cavity (*5*), whereas the H-site in hGSTP1-1 is half-hydrophobic and half-hydrophilic with functionally important water molecules (*4*).

Benzo[*a*]pyrene (BP) is the prototype of the polycyclic aromatic hydrocarbon family of environmental carcinogens,

[†] This work was supported in part by Grants ES09140 (S.V.S. and P.Z.) and ES07804 (P.Z.) from the National Institute of Environmental Health Sciences, NIH, and by the National Cancer Institute, NIH, DHHS, under contract with ABL (X.J.). The contents of this publication do not necessarily reflect the views or policies of the Department of Health and Human Services (DHHS), nor does mention of trade names, commercial products, or organizations imply endorsement by DHHS or the United States Government.

[‡] The coordinates and structure factors have been deposited with the Protein Data Bank. The accession codes are 3pgt and 4pgt.

* Address correspondence to this author: phone (301) 846-5035; fax (301) 846-6073; e-mail jix@ncifcrf.gov. Postal address: NCI−FCRDC, P.O. Box B, Frederick, MD 21702.

[§] National Cancer Institute−Frederick Cancer Research and Development Center.

[∥] Mercy Hospital of Pittsburgh.

[⊥] University of Arkansas for Medical Sciences.

[1] Abbreviations: GSH, glutathione; GST, GSH *S*-transferase; *x*GSTY*m*-*n*, class Y (A, α; M, μ; P, π; S, σ) GST with subunit type *m*-*n* (*m* and *n* = 1, 2, ...) from *x* (m, murine; h, human; r, rat; s, squid; b, bovine); SjGST, GST from *Schistosoma japonicum*; BP, benzo[*a*]pyrene; (+)-*anti*-BPDE, (+)-*anti*-7,8-dihydroxy-9,10-oxy-7,8,9,10-tetrahydrobenzo[*a*]pyrene; GSBpd, GSH conjugate of (+)-*anti*-BPDE.; GSHex, *S*-hexylglutathione; GSPhen, 9-(*S*-glutathionyl)-10-hydroxy-9,10-dihydrophenanthrene; GSEa, GSH conjugate of ethacrynic acid; G-site, GSH-binding site; H-site, xenobiotic substrate-binding site; Hepes, *N*-(2-hydroxethyl)piperazine-*N*'-(2-ethanesulfonic acid); Mes, 2-(*N*-morpholino)ethanesulfonic acid; rms, root mean square.

10.1021/bi990668u CCC: $18.00
Published on Web 07/22/1999

Scheme 1

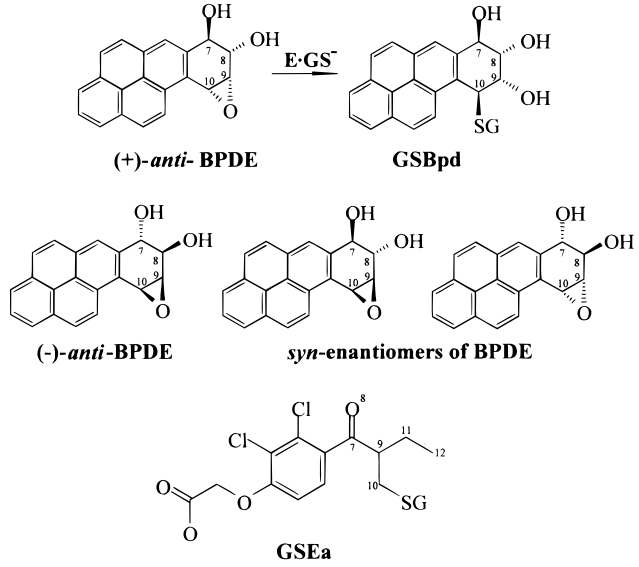

which are abundant in cigarette smoke, automobile exhaust, etc. The ultimate carcinogen of BP is believed to be its diol epoxide, 7,8-dihydroxy-9,10-oxy-7,8,9,10-tetrahydrobenzo-[*a*]pyrene (BPDE) (*6*−*8*). BPDE exists as a pair of diastereomers (*syn* and *anti*), and each diastereomer can be resolved into a pair of optical enantiomers (Scheme 1) (*7*). Of the four isomers, (+)-*anti*-BPDE has been shown to be the most potent carcinogen in experimental animals in vivo (*7*, *9*). A critical event in BP-induced carcinogenesis is that the electrophilic epoxide center of *anti*-BPDE can be the site of nucleophilic attack by nucleophilic sites in DNA. Alternatively, several different pathways of biotransformation of *anti*-BPDE can convert this compound to less electrophilic metabolites and can therefore protect DNA. The toxicologically most important metabolic pathway of *anti*-BPDE is its hGSTP1-1-catalyzed conjugation with GSH (Scheme 1) (*10*), and the enzyme is enantioselective toward BPDE (*11*). Because the H-site in class π GSTs has both a hydrophobic region and a hydrophilic region (*4*), we proposed that the BPDE ring system interacts with the hydrophobic region of the H-site and the hydroxyl groups of BPDE with the hydrophilic region, which could stabilize the reaction intermediate (*11*). A three-dimensional structure of hGSTP1-1 complexed with the product of GSH addition to BPDE should shed light on the structural basis for the enantioselectivity of the enzyme.

Four allelic forms of hGSTP1-1 have been identified in the human population (*12*−*15*). These variants are the result of polymorphism in positions 104 (either I104 or V104) and 113 (either A113 or V113). Residue 104 within the H-site residue has been the subject of in-depth structural, enzymological, and mutagenesis studies (*4*, *11*, *16*−*18*). Residue 113 is located at the tip of a helix−turn−helix motif (the opening of the solvent channel between the two subunits) and is more than 20 Å away from the active center. The four variants of hGSTP1-1 have significantly different specific activities and affinities for (+)-*anti*-BPDE (*19*) and other xenobiotic substrates (*20*). For example, the turnover number of isoform hGSTP1-1[V104] with (+)-*anti*-BPDE is significantly higher (3.4-fold) than that of isoform hGSTP1-1[I104] (*11*). The higher activity of the V104 versus I104 form also holds for the V104/V113−I104/V113 pair of enzymes, albeit to a lesser degree (*19*). To elucidate the roles of residues 104 and 113 in the catalytic efficiency of the hGSTP1-1-catalyzed GSH conjugation reaction of (+)-*anti*-BPDE, three-dimensional structures are essential. Here, we report the crystal structures of the GSH conjugate of (+)-*anti*-BPDE (GSBpd) in complex with hGSTP1-1[I104] and with hGSTP1-1[V104]. When not specified, the enzyme contains residue Ala at position 113.

Table 1: Summary of Data Collection for the Complexes hGSTP1-1[I104]·GSBpd and hGSTP1-1[V104]·GSBpd

complex	hGSTP1-1[I104]·GSBpd	hGSTP1-1[V104]·GSBpd
D_{min} (Å)	2.14	2.10
redundancy	8.61	15.0
overall completeness (%)	92.7	90.8
overall $I/\sigma(I)$	24.0	11.2
last shell completeness (%)	83.2	81.0
last shell $I/\sigma(I)$	7.7	4.5
$R_{scaling}$[a]	0.05	0.06

[a] $R_{scaling} = \sum|I - \langle I\rangle|/\sum I$. Friedel pairs were merged.

EXPERIMENTAL PROCEDURES

Sample Preparation. The hGSTP1-1[I104] and -[V104] variants were expressed and purified as described previously (*20*). Briefly, for the V104 variant, position +313 (relative to the start codon) in the cDNA encoding hGSTP1-1[I104] was mutated (A to G) to replace the Ile codon with a triplet encoding Val. The mutated cDNA was subcloned into the bacterial expression vector pET9a (Novagen), and the hGSTP1-1[V104] protein was expressed in *Escherichia coli* BL21(DE3)pLysS and purified to homogeneity by GSH affinity chromatography (*21*). GSBpd was synthesized and purified as previously described (*22*).

Crystallization and X-ray Diffraction Data Collection. Crystals of hGSTP1-1[I104]·GSBpd were grown in hanging drops that initially consisted of 4.3 mg/mL protein in 50 mM 2-(*N*-morpholino)ethanesulfonic acid (Mes) buffer (pH 6.5) containing 0.5 mM GSBpd, 5 mM cobalt chloride hexahydrate, and 0.9 M ammonium sulfate. The drops were equilibrated at room temperature against well solutions containing 1.8 M ammonium sulfate and 10 mM cobalt chloride hexahydrate in 0.1 M Mes buffer (pH 6.5) (Hampton Crystal Screen II, no. 25). However, the crystallization conditions mentioned above were not appropriate for the V-104 form of the protein. Crystals of hGSTP1-1[V104]·GSBpd were obtained in hanging drops containing 4.3 mg/mL protein, 0.55 mM GSBpd, and 0.8 M ammonium sulfate in 50 mM Mes buffer (pH 6.0) and equilibrated with 1.6 M ammonium sulfate in 0.1 M Mes buffer (pH 6.0). Both complexes crystallized in the C2 space group with unit cell parameters $a = 78.15$ Å, $b = 89.74$ Å, $c = 68.68$ Å, $\alpha = \gamma = 90°$, and $\beta = 97.72°$. X-ray diffraction data were collected from single crystals by using a MacScience DIP2020 image plate system with an Enraf Nonius FR501 rotating anode (Cu Kα radiation) X-ray source operated at 45 kV/110 mA. An Oxford low-temperature system was used to maintain the data crystal at 100 K. The cryoprotectant used was 25% glycerol, and the distance from data crystal to detector was 105 mm. The raw data images were processed and scaled

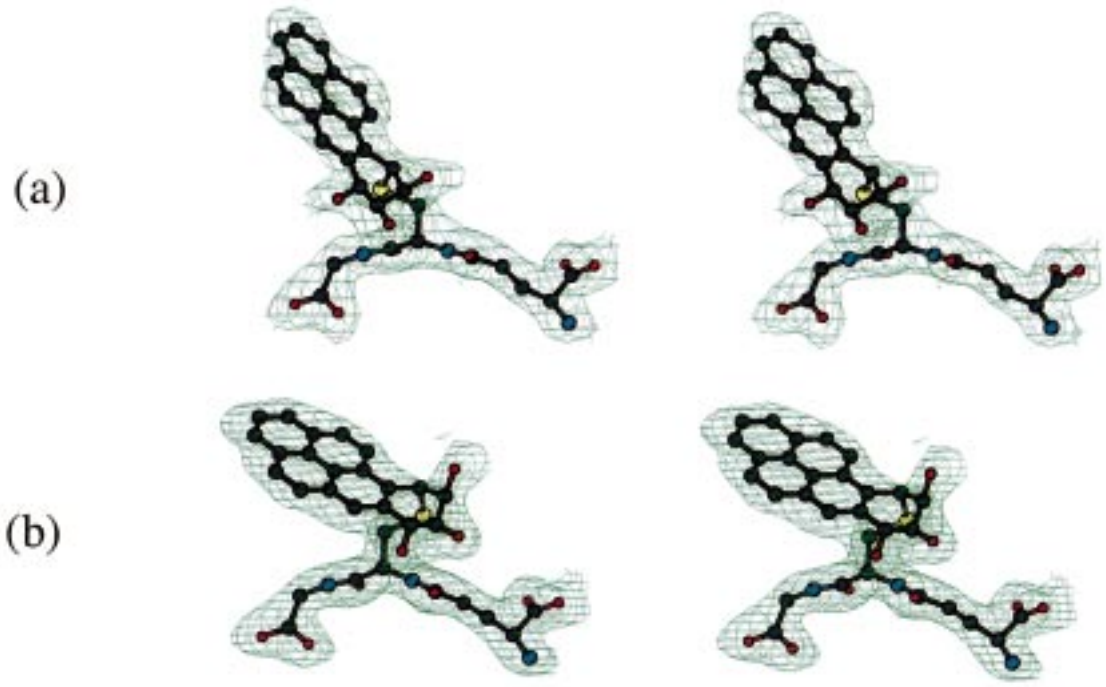

FIGURE 1: Stereoview of final ($2F_o - F_c$) maps, contoured at 1σ, of the product molecules GSBpd in complex with (a) hGSTP1-1[I104] and (b) hGSTP1-1[V104]. The product molecules are represented by ball-and-stick models with carbon in black, oxygen in red, nitrogen in blue, and sulfur in yellow. The electron density is displayed as a green net.

on a Silicon Graphics Indigo2 computer with a Solid Impact graphics system using the HKL2000 suite of programs (*23*). Data collection statistics are summarized in Table 1.

Crystal Structure Determination and Refinement. The crystal structures of hGSTP1-1[I104]·GSBpd and hGSTP1-1[V104]·GSBpd were determined with the difference Fourier technique. The starting model was the 1.8 Å structure of hGSTP1-1[V104] in complex with *S*-hexylglutathione (GSHex) (*4*) with the hexyl groups of GSHex and solvent molecules removed. Initial refinement was carried out with the X-PLOR (*24*) package. V104 was replaced by I104 for hGSTP1-1[I104]·GSBpd according to the difference Fourier maps contoured at 3σ and -3σ. Further refinement was carried out with the program suite SHELXL-97 (*25*). The crystallographic *R*-factor for the final model of hGSTP1-1[I104]·GSBpd was 0.16 for all the reflections between 20.0 and 2.14 Å resolution, which, after the inhibitor and water molecules were removed, was used as the starting model for the refinement of hGSTP1-1[V104]·GSBpd. The final *R*-factor was 0.19 for X-ray diffraction data between 20.0 and 2.10 Å resolution. The O program suite (*26*) was used on a Silicon Graphics Indigo2 computer with a Solid Impact graphics system for model building and adjustments.

The entire model was checked and adjusted after each cycle of refinement. Complete models of the GSBpd molecules were built into the difference Fourier map contoured at 2σ. The final $2F_o - F_c$ electron density maps for GSBpd in the two complexes are shown in Figure 1. The corresponding omit maps (not shown) have similar quality. Mes molecules were built into the difference electron density contoured at $+2.0\sigma$ without any ambiguity. Water molecules were located in the difference Fourier maps as peaks higher than 3σ. After all identifiable water molecules were found, they were verified by a series of omit maps (*27*) with a set of 100 molecules deleted each time. This procedure was performed in ascending order starting from the bottom of the list of water molecules ranked according to the parameter OCC^2/B (*28*), the ratio of the square of the fractional occupancy factor (OCC) of the oxygen atom position and the crystallographic temperature factor (*B*). All X-ray diffraction data were included in electron density map calculations. A summary of the crystallographic refinement is shown in Table 2.

RESULTS AND DISCUSSION

Overall Structure. Figure 2 schematically illustrates the structures of hGSTP1-1[I104]·GSBpd and hGSTP1-1[V104]·GSBpd. The final model of hGSTP1-1[I104]·GSBpd includes 419 amino acid residues, 2 GSBpd molecules, 4 Mes molecules, 7 sulfate anions, and 491 water molecules. The final model of hGSTP1-1[V104]·GSBpd includes 419 amino acid residues, 2 GSBpd molecules, 2 Mes molecules, 2 sulfate anions, and 427 water molecules (Table 2). The crystallographic *R*-factor for all X-ray diffraction data is 0.156 for the I104 complex and 0.191 for the V104 complex. Both structures have good geometry with the root mean square (rms) deviations for bond distances of 0.006 and 0.004 Å, respectively (Table 2). More than 93% of the residues exhibit the most favorable $\phi-\psi$ relationship according to the protein structure verification procedure PROCHECK (*29*). The structures of the two hGSTP1-1·GSBpd complexes are quite similar except in the immediate vicinity of the active site. The rms deviation for all 419 Cα atoms between the two dimeric molecules is 0.26 Å. This rms value decreases to 0.19 Å when 14 pairs of Cα atoms are excluded from the optimized alignment. The fold of the polypeptide chain (Figure 2) is virtually the same as that reported previously (*30*). Each subunit contains two domains, a smaller α/β-domain and a larger α-domain (Figure 2). The α/β-domain consists of 80 amino acid residues that form the secondary-

Table 2: Summary of the Least-Squares Refinement Statistics for the Complexes hGSTP1-1[I104]·GSBpd and hGSTP1-1[V104]·GSBpd

complex	hGSTP1-1[I104]·GSBpd	hGSTP1-1[V104]·GSBpd
resolution range (Å)[a]	20.0−2.14	20.0−2.10
no. of reflections used	23832	25549
crystallographic *R*-factor[b]		
$I \geq 2\sigma(I)$	0.155	0.180
all data	0.156	0.191
no. of amino acid residues	419[c]	419[c]
ligand molecules	2 GSBpd and 4 Mes	2 GSBpd and 2 Mes
solvent molecules	7 SO_4^{2-} and 491 H_2O	2 SO_4^{2-} and 427 H_2O
rmsd from ideal distances (Å)		
bond distances	0.006	0.004
angle distances	0.020	0.017

[a] Data used for refinement. [b] The crystallographic *R*-factor $= \sum_{hkl}||F_o| - |F_c||/\sum_{hkl}|F_o|$. [c] A methionine residue was observed at the N-terminus of one subunit.

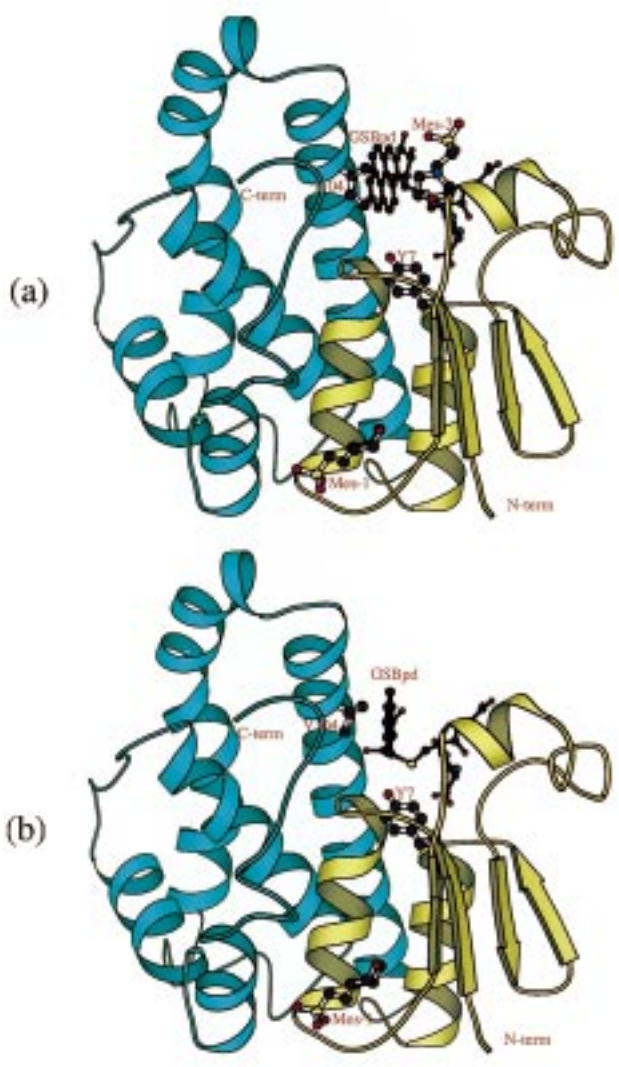

FIGURE 2: Schematic representations of one subunit of (a) hGSTP1-1[I104]·GSBpd and (b) hGSTP1-1[V104]·GSBpd. The N-terminal α/*β*-domain is in yellow, and the C-terminal α-domain is in blue. The product complex GSBpd is shown as a filled ball-and-stick model, and the Mes molecules and the side chains of Y7 and I/V104 are shown as open ball-and-stick models. The atomic color scheme is shown with carbon in black, oxygen in red, nitrogen in blue, and sulfur in yellow.

structure elements *β*2, α1, *β*1, α2, *β*3, *β*4, and α3. The α-domain contains five α-helices (α4 to α8). The initiator methionine in subunit A is involved in intermolecular interactions with symmetry-related molecules, causing this methionine to assume a defined conformation that is observed in the electron density map. However, it is not seen at the N-terminus of subunit B. The orientation of the Bpd moiety of the product molecule assumes significantly different orientations in the two complex structures (Figures 2 and 3a). Mes-1, the Mes molecule that is located in a potential non-substrate-binding site (*4*), is found in both complexes. However, Mes-2, the Mes molecule found between the Bpd moiety and the α2-helix in hGSTP1-1[I104]·GSBpd, is not observed in hGSTP1-1[V104]·GSBpd.

Enantioselectivity of hGSTP1-1 toward anti-BPDE. As we reported previously, the H-site in hGSTP1-1 is half-hydrophobic and half-hydrophilic (*4*). Five H-site water molecules form a hydrogen bond network with R13 and N204, NE(R13)···Wat1···Wat2···Wat3···OD1(N204)···Wat4···Wat5, which extends into a solvent channel that leads to the surface of the protein via Wat4 (*4*) and connects with the bulk solvent between the two subunits via Wat1 (not shown). These water molecules have also been found in various hGSTP1-1 complexes (*31*). We proposed that the five water molecules, together with R13 and N204, make up the hydrophilic portion of the H-site, which preferentially interacts with the hydrophilic groups of the xenobiotic substrate whenever feasible (*4*). On the basis of the fact that hGSTP1-1 favors (+)-*anti*-BPDE over (−)-*anti*-BPDE (*10*) and the results of our molecular modeling studies, we proposed that the polycyclic ring system of the Bpd moiety prefers the interaction with the hydrophobic portion of the H-site and the hydroxyl groups of the Bpd moiety prefer the interaction with the hydrophilic portion of the H-site (*11*). This is indeed the case. The GSBpd molecule described here is the GSH conjugate of (+)-*anti*-BPDE. The electron density maps of the product complexes in the active site (Figure 1) indicate that the binding modes of GSBpd are well defined. Although the exact position of the Bpd moiety is not the same in the two complex structures, the polycyclic ring system of Bpd interacts with the hydrophobic portion of the H-site and the hydroxyl groups of Bpd interact with the hydrophilic portion of the H-site in both complexes (Figure 3a). For (−)-*anti*-BPDE, the interactions between the H-site and the substrate will be exactly the opposite and, therefore, are energetically unfavorable (*11*). In conclusion, the enantioselectivity of hGSTP1-1 toward anti-BPDE is one of the consequences of the half-hydrophobic and half-hydrophilic nature of the H-site.

Binding Modes of GSBpd in hGSTP1-1[I104] and hGSTP1-1[V104]. The product molecule GSBpd assumes

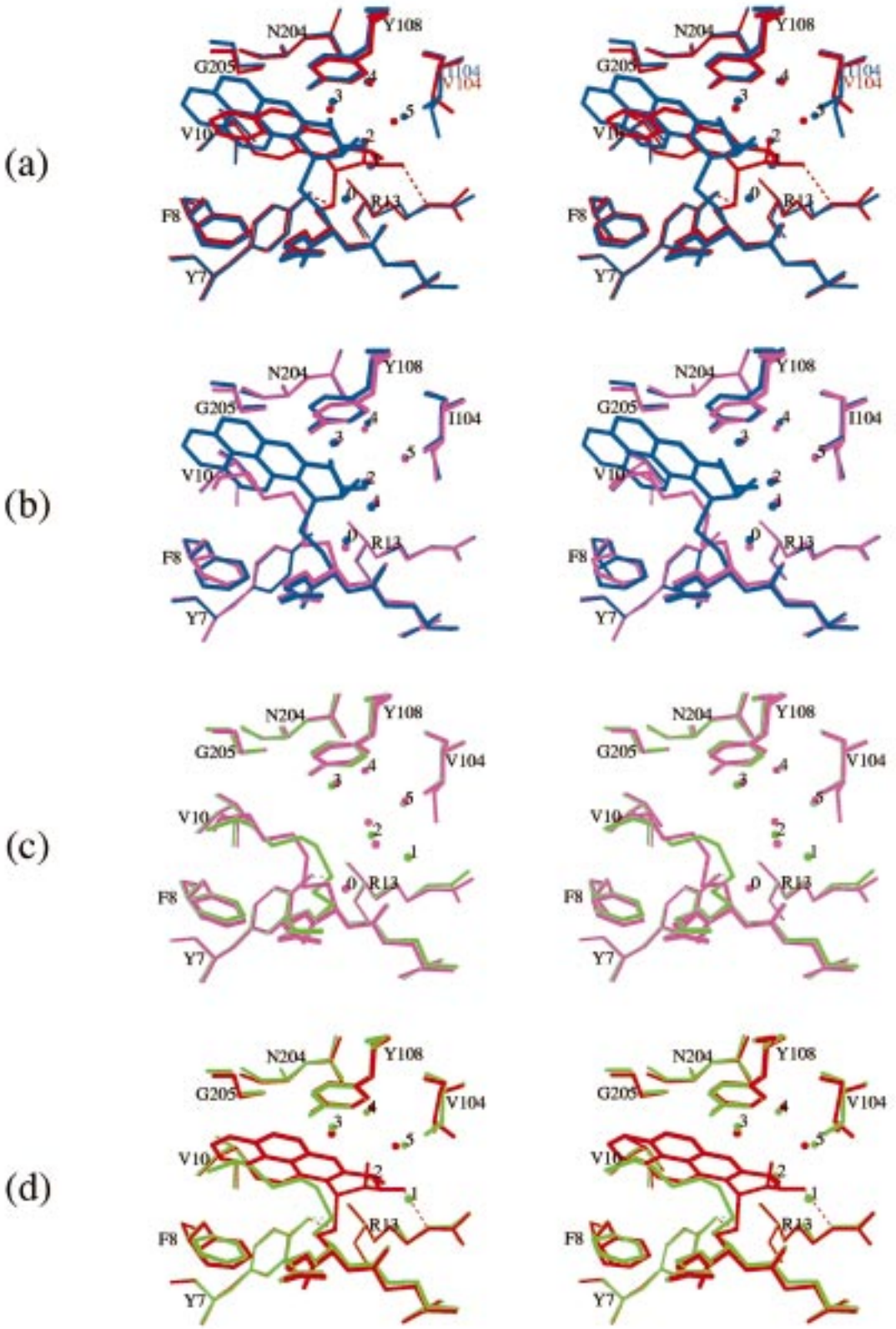

FIGURE 3: Stereoview of a stick model of the H-site of (a) hGSTP1-1[I104]·GSBpd (blue, this work) compared with hGSTP1-1[V104]·GSBpd (red, this work), (b) hGSTP1-1[I104]·GSBpd (blue, this work) with hGSTP1-1[I104]·GSHex [purple (*31*)], (c) hGSTP1-1[V104]·GSHex [green (*4*)] with hGSTP1-1[I104]·GSHex [purple (*31*)], and (d) hGSTP1-1[V104]·GSBpd (red, this work) with hGSTP1-1[V104]·GSHex [green (*4*)]. The H-site-defining residues are labeled. The H-site water molecules are illustrated as balls and are labeled numerically from 0 to 5.

significantly different binding modes in the two complex structures (Figure 3a). The two binding modes have four significant differences: the conformation of residue 104, the position of the Bpd moiety, the position of the sulfur atom of the GS moiety, and the H-site water structure. In both complexes, the shortest distance between the Bpd moiety

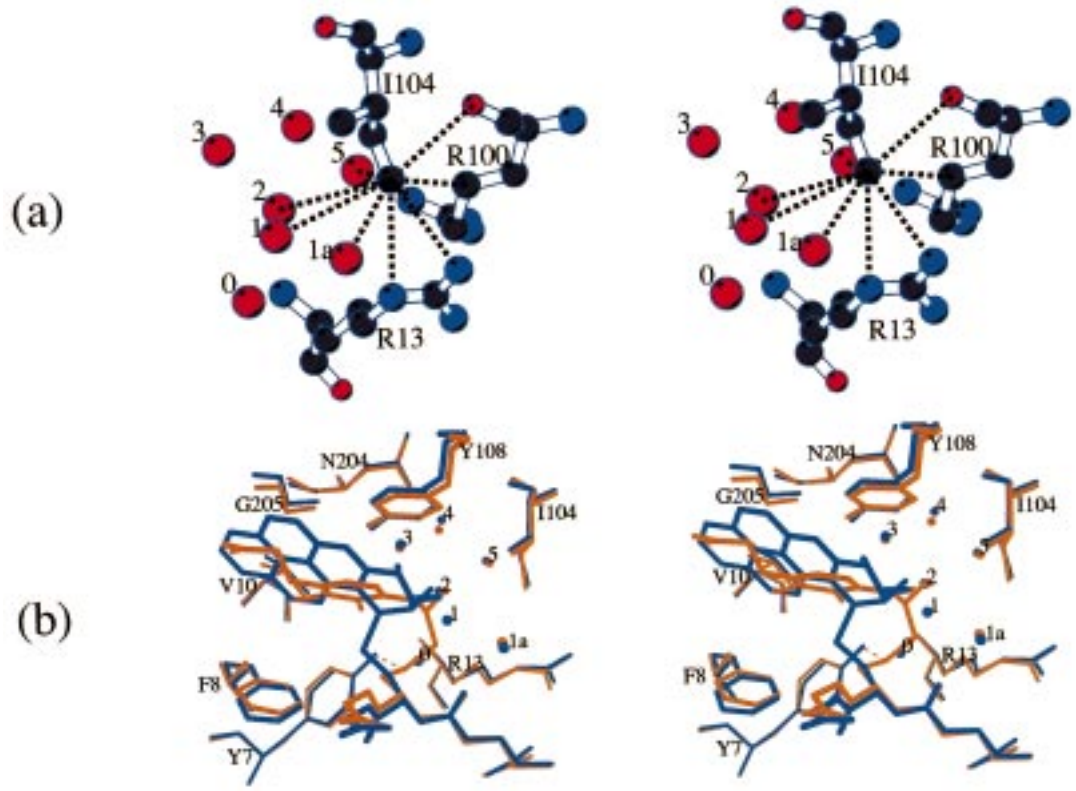

FIGURE 4: Stereoview of (a) a ball-and-stick model showing the interaction of I104 and its surrounding atoms in the H-site of hGSTP1-1[I104]·GSBpd (this work) and (b) a stick model of the H-site of hGSTP1-1[I104]·GSBpd (blue, this work) compared with that of hGSTP1-1[I104]·GSEa [yellow (*32*)]. The H-site-defining residues are labeled. The atomic color scheme is shown in (a) with carbon in black, oxygen in red, and nitrogen in blue. H-site-bound water molecules are illustrated as balls and are labeled numerically from 0 to 5 with the addition of Wat1a, which connects the H-site water structure with the bulk solvent in the solvent channel at the dimer interface.

and residue 104 is ~4.0 Å. Two electrostatic interactions are observed in hGSTP1-1[V104]·GSBpd, including the hydrogen bond between the hydroxyl group of Y7 and the sulfur atom of GSH (3.2 Å) and that between atom NE of R13 and the hydroxyl group at position 8 (Scheme 1) of the Bpd moiety (3.0 Å) (Figure 3a). These two hydrogen bonds are functionally relevant, because it is well accepted that both Y7 and R13 participate in GST catalysis. In the hGSTP1-1[I104] complex, however, both hydrogen bonds are broken due to a positional shift of the Bpd moiety toward the hydrophobic half of the H-site by ~2.5 Å. The unsaturated electrostatic potential of the hydroxyl group of Y7 is neutralized by the introduction of one more water molecule into the H-site (Wat0 in Figure 3a). This water molecule is also observed in hGSTP1-1[I104]·GSHex where the hydrogen bond between the hydroxyl group of Y7 and the sulfur atom of GSHex is broken as well (Figure 3b) (*31*). It appears that this particular position in the H-site is occupied at any given time either by the sulfur atom of GSH or by a water molecule. With the addition of Wat0, the number of H-site water molecules in hGSTP1-1[I104]·GSBpd is six (Figure 3a). On the contrary, in hGSTP1-1[V104]·GSBpd, two of the five H-site water molecules are displaced by the Bpd moiety (Figure 3a). It appears that water molecules 3, 4, and 5 are conserved in both complex structures and that water molecules 0, 1, and 2 are displaceable, depending on the substrate-binding mode. Although the product-binding mode is not necessarily the substrate-binding mode, the relative positions and interactions with the H-site of the sulfur atom of the GS moiety and the electrophilic center of the Bpd moiety observed in the hGSTP1-1[V104]·GSBpd complex suggest a proper alignment between the reactive centers on the two substrate molecules GSH and (+)-*anti*-BPDE. Given that hGSTP1-1[V104] is indeed more active than hGSTP1-1[I104] toward (+)-*anti*-BPDE (*11*, *19*), residue 104 must be the determining factor for the differential activity of the two hGSTP1-1 variants.

I104 Does Not Have Conformational Freedom, Whereas V104 Does. In the structures of hGSTP1-1[I104]·GSBpd (this work) and hGSTP1-1[I104]·GSHex (*31*), I104 has an almost identical conformation (Figure 3b), where the CD methyl group is surrounded by eight atoms, including NE and NH2 of R13, O and CG of R100, Wat1a, Wat1, Wat2, and Wat5 (Figure 4a). Wat1a bridges the H-site water network and the bulk solvent in the channel between the two subunits and is also hydrogen bonded to atom NE of R13 (not shown). The distances from the CD atom of I104 to the eight atoms listed above range from 3.5 to 4.0 Å. Such an arrangement appears to prohibit any significant conformational change of I104. When the H-site water molecules 0, 1, and 2 are displaced by the substrate/product, the CD atom of I104 interacts directly with the substrate/product. For example, in hGSTP1-1[I104]·GSEa (*32*), the CD atom of I104 is still surrounded by eight atoms, where Wat1 and Wat2 are replaced by C11 and C12 of GSEa (Figure 4b and Scheme 1). The same conformation of I104 has also been found in the complexes of hGSTP1-1[I104] with other product molecules, such as γ-glutamyl(*S*-benzylcysteinyl)-D-phenylglycine (*31*), *p*-(bromobenzyl)glutathione (*33*), and the Meisenheimer complex (*33*). No other conformation of I104 has been reported.

We have observed two distinct conformations of V104. It assumes the same conformation as I104 around the CA−CB bond when the xenobiotic portion of the product is GSHex and 9-(*S*-glutathionyl)-10-hydroxy-9,10-dihydrophenanthrene (GSPhen) (*4*), whereas it assumes a significantly different conformation in the hGSTP1-1[V104]·GSBpd complex (this work). In hGSTP1-1[V104]·GSHex, the fork of V104 points toward the H-site, whereas in hGSTP1-1[V104]·GSBpd, it points away (Figure 3d). Without this conformational change, the shortest distance between V104 and the Bpd moiety would be ∼3.0 Å in hGSTP1-1[V104]·GSBpd. It is therefore suggested that the fork of V104 points toward the H-site when the xenobiotic substrate is small and it points away to accommodate a larger substrate such as BPDE, so that the electrophilic center of BPDE may be properly positioned relative to the sulfur atom of GSH. Provided that the BPDE molecule binds to the H-site in the same way that GSBpd does, the electrophilic center of the BPDE molecule is aligned perfectly with the sulfur atom of the GSH molecule and Y7, and R13 may be able to participate in catalysis as expected. We propose that the binding model of GSBpd as seen in hGSTP1-1[I104]·GSBpd is possible for hGSTP1-1[V104] on the basis of the following three reasons. First, different binding modes of GSBpd do not cause significant conformational changes of the H-site and the protein. Second, it is reasonable for a particular substrate and/or product to have two binding modes to the same binding site with catalytically different properties. Third, two binding modes for GSEa have been observed in the H-site of hGSTP1-1[I104] (*32*).

Residue 104 and Substrate Specificity. As seen in all the complex structures discussed above, the shortest distance between residue 104 and the xenobiotic moiety is ∼4.0 Å. Prohibited by the steric interaction with I104, the sulfur atom of GSH may not be properly aligned with the electrophilic center of BPDE in the active center of hGSTP1-1[I104] and the catalytically relevant interactions between the substrates and Y7 and R13 may not be easily achievable. In contrast, the conformational freedom of V104 makes it possible for BPDE to be properly bound to hGSTP1-1[V104] (Figure 3a). Only for certain xenobiotic substrates (such as ethacrynic acid, which is smaller than BPDE) is it possible for hGSTP1-1[I104] to achieve catalytically preferred binding where the distance between the hydroxyl group of Y7 and the sulfur atom of GSH is within 3.5 Å and atom O8 may interact with R13 via Wat1a (Figure 4b and Scheme 1). It appears that hGSTP1-1[V104] has a broader substrate specificity than the I104 variant.

H-Site Water Structure. From the comparison between the structures of hGSTP1-1[V104]·GSHex at 1.8 Å resolution (*4*) and hGSTP1-1[I104]·GSHex at 2.8 Å resolution (*30*), it seems that the additional methyl group, present in the I104 but absent in the V104 form of the enzyme, causes the positional shift of water molecules 1 to 4 and the displacement of Wat5 (*4*). However, in the 2.0 Å resolution structure of hGSTP1-1[I104]·GSHex (*31*) and that of hGSTP1-1[I104]·GSBpd (this work), all five H-site water molecules are observed. In addition, one extra water molecule (Wat0) is introduced into the H-site to occupy the space vacated by the sulfur atom (Figure 3b). A revised comparison between hGSTP1-1[I104]·GSHex (*31*) and hGSTP1-1[V104]·GSHex (*4*) reveals that the positional shifts occur only for Wat1 and Wat2 (Figure 3c). The xenobiotic moiety of the product molecule causes much more significant disturbance to the H-site water structure than I104 does in two respects. First, the position of the sulfur atom of GSH dictates the existence of Wat0 (Figure 3a,c). Second, the xenobiotic moiety may displace water molecules depending on where it binds. Therefore, it is evident that the H-site water structure functions to mediate substrate−protein interactions and that the increase or decrease in the H-site water molecules depends on the binding mode of a particular substrate molecule.

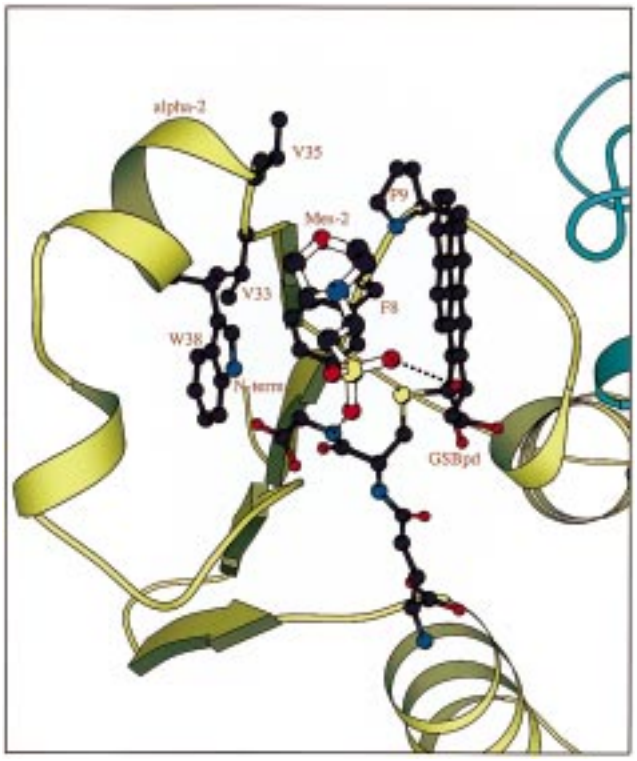

FIGURE 5: Schematic representations showing the location of the Mes-2 molecule found in hGSTP1-1[I104]·GSBpd. The N-terminal α/β-domain is in yellow, and the C-terminal α-domain is in blue. The product complex GSBpd and the side chains of F8, P9, V33, V35, and V38 are shown as filled ball-and-stick models. The Mes-2 molecule is shown as an open ball-and-stick model. The atomic color scheme is shown with carbon in black, oxygen in red, nitrogen in blue, and sulfur in yellow. All illustrations in Figures 1−5 were prepared with Molscript (*36*).

Mes-Binding Sites. Mes-1 is bound in a cavity (Figure 2). Similarly, an *N*-(2-hydroxethyl)piperazine-*N*'-2-ethanesulfonic acid (Hepes) molecule was found in both hGSTp1-1[V104]·GSHex and hGSTp1-1[V104]·GSPhen (*4*). This binding site has also been identified in other hGSTP1-1 complexes (*31*, *33*). The bottom of the cavity is a hydrophobic surface, and several potential hydrogen bond donor and acceptor groups are located on the edge of the cavity. Covering the hydrophobic bottom of the cavity, Mes-1 forms a similar number of hydrogen bonds with the protein as Hepes does. It has been proposed that the Mes-1-binding site is potentially a non-substrate-binding site (*4*, *33*). However, the hypothesis has not yet been proved.

In addition to Mes-1, another Mes-binding site was identified (*31*). This site was located at the bottom of the dimer interface and was not fully occupied. We suggest that this Mes-binding site is virtually the potential transport

binding site identified previously in sGSTS1-1 (*34*) and in SjGST (*35*). We have identified, in hGSTP1-1[I104]·GSBpd, the Mes-2-binding site, which is located between the α2-helix and the Bpd moiety of the product (Mes-2, Figure 2a), immediately above the four-stranded β-sheet. The sulfonic acid moiety of Mes-2 forms two hydrogen bonds with GSBpd, and the ring system is surrounded by hydrophobic side chains of F8, P9, V33, V35, and W38 and the polycyclic ring system of GSBpd (Figure 5). Although there is no Mes found at this position in hGSTP1-1[V104]·GSBpd, the alignment using all Cα atoms of one subunit reveals no significant shift of the α2-helix. It appears that hGSTP1-1 has a well-defined H-site that is much more spacious than previously assumed.

Conclusions. The crystal structures of hGSTP1-1[I104]·GSBpd and hGSTP1-1[V104]·GSBpd reveal that the half-hydrophilic and half-hydrophobic nature of the H-site is responsible for the enantioselectivity of hGSTP1-1 for (+)-*anti*-BPDE over (−)-*anti*-BPDE. The binding mode of the product of GSH conjugation of (+)-*anti*-BPDE is significantly different in hGSTP1-1[I104] as compared with hGSTP1-1[V104] due to the lack of conformational freedom of I104. V104 is able to assume two distinct conformations depending on the size and shape of the xenobiotic substrate. It appears that hGSTP1-1[V104] has a broader substrate specificity than the I104 variant of the enzyme. The H-site water structure functions to mediate substrate−protein interaction and thus facilitates the hGSTP1-1-catalyzed GSH conjugation reaction.

REFERENCES

1. Armstrong, R. N. (1991) *Chem. Res. Toxicol. 4*, 131−140.
2. Armstrong, R. N. (1994) *Adv. Enzymol. Relat. Areas Mol. Biol. 69*, 1−44.
3. Armstrong, R. N. (1997) *Chem. Res. Toxicol. 10*, 2−18.
4. Ji, X., Tordova, M., O'Donnell, R., Parsons, J. F., Hayden, J. B., Gilliland, G. L., and Zimniak, P. (1997) *Biochemistry 36*, 9690−9702.
5. Ji, X., Johnson, W. W., Sesay, M. A., Dickert, L., Prasad, S. M., Ammon, H. L., Armstrong, R. N., and Gilliland, G. L. (1994) *Biochemistry 33*, 1043−1052.
6. Thakker, D. R., Yagi, H., Levin, W., Wood, A. W., Conney, A. H., and Jerina, D. M. (1985) in *Bioactivation of Foreign Compounds* (Anders, M. W., Ed.) pp 177−242, Academic Press, New York.
7. Buening, M. K., Wislocki, P. G., Levin, W., Yagi, H., Thakker, D. R., Akagi, H., Koreeda, M., Jerina, D. M., and Conney, A. H. (1978) *Proc. Natl. Acad. Sci. U.S.A. 75*, 5358−5361.
8. Gelboin, H. V. (1980) *Physiol. Rev. 60*, 1107−1166.
9. Slaga, T. J., Bracken, W. J., Gleason, G., Levin, W., Yagi, H., Jerina, D. M., and Conney, A. H. (1979) *Cancer Res. 39*, 67−71.
10. Robertson, I. G., Guthenberg, C., Mannervik, B., and Jernstrom, B. (1986) *Cancer Res. 46*, 2220−2224.
11. Hu, X., O'Donnell, R., Srivastava, S. K., Xia, H., Zimniak, P., Nanduri, B., Bleicher, R. J., Awasthi, S., Awasthi, Y. C., Ji, X., and Singh, S. V. (1997) *Biochem. Biophys. Res. Commun. 235*, 424−428.
12. Ahmad, H., Wilson, D. E., Fritz, R. R., Singh, S. V., Medh, R. D., Nagle, G. T., Awasthi, Y. C., and Kurosky, A. (1990) *Arch. Biochem. Biophys. 278*, 398−408.
13. Harries, L. W., Stubbins, M. J., Forman, D., Howard, G. C., and Wolf, C. R. (1997) *Carcinogenesis 18*, 641−644.
14. Ali-Osman, F., Akande, O., Antoun, G., Mao, J. X., and Buolamwini, J. (1997) *J. Biol. Chem. 272*, 10004−10012.
15. Watson, M. A., Stewart, R. K., Smith, G. B., Massey, T. E., and Bell, D. A. (1998) *Carcinogenesis 19*, 275−280.
16. Hu, X., Ji, X., Srivastava, S. K., Xia, H., Awasthi, S., Nanduri, B., Awasthi, Y. C., Zimniak, P., and Singh, S. V. (1997) *Arch. Biochem. Biophys. 345*, 32−38.
17. Johansson, A. S., Stenberg, G., Widersten, M., and Mannervik, B. (1998) *J. Mol. Biol. 278*, 687−698.
18. Sundberg, K., Johansson, A. S., Stenberg, G., Widersten, M., Seidel, A., Mannervik, B., and Jernstrom, B. (1998) *Carcinogenesis 19*, 433−436.
19. Hu, X., Xia, H., Srivastava, S. K., Herzog, C., Awasthi, Y. C., Ji, X., Zimniak, P., and Singh, S. V. (1997) *Biochem. Biophys. Res. Commun. 238*, 397−402.
20. Zimniak, P., Nanduri, B., Pikula, S., Bandorowicz-Pikula, J., Singhal, S. S., Srivastava, S. K., Awasthi, S., and Awasthi, Y. C. (1994) *Eur. J. Biochem. 224*, 893−899.
21. Simons, P. C., and Vander Jagt, D. L. (1977) *Anal. Biochem. 82*, 334−341.
22. Hu, X., Srivastava, S. K., Xia, H., Awasthi, Y. C., and Singh, S. V. (1996) *J. Biol. Chem. 271*, 32684−32688.
23. Otwinowski, Z., and Minor, W. (1997) *Methods Enzymol. 276*, 307−326.
24. Brünger, A. T., and Rice, L. M. (1997) *Methods Enzymol. 277*, 243−269.
25. Sheldrick, G. M., and Schneider, T. R. (1997) *Methods Enzymol. 277*, 319−343.
26. Jones, T. A., and Kjeldgaard, M. (1997) *Methods Enzymol. 277*, 173−208.
27. Bhat, T. N. (1988) *J. Appl. Crystallogr. 21*, 279−281.
28. James, M. N., and Sielecki, A. R. (1983) *J. Mol. Biol. 163*, 299−361.
29. Laskowski, R. A., MacArthur, M. W., Moss, D. S., and Thornton, J. M. (1993) *J. Appl. Crystallogr. 26*, 283−291.
30. Reinemer, P., Dirr, H. W., Ladenstein, R., Huber, R., Lo Bello, M., Federici, G., and Parker, M. W. (1992) *J. Mol. Biol. 227*, 214−226.
31. Oakley, A. J., Lo Bello, M., Battistoni, A., Ricci, G., Rossjohn, J., Villar, H. O., and Parker, M. W. (1997) *J. Mol. Biol. 274*, 84−100.
32. Oakley, A. J., Lo Bello, M., Mazzetti, A. P., Federici, G., and Parker, M. W. (1997) *FEBS Lett. 419*, 32−36.
33. Prade, L., Huber, R., Manoharan, T. H., Fahl, W. E., and Reuter, W. (1997) *Structure 5*, 1287−1295.
34. Ji, X., von Rosenvinge, E. C., Johnson, W. W., Armstrong, R. N., and Gilliland, G. L. (1996) *Proc. Natl. Acad. Sci. U.S.A. 93*, 8208−8213.
35. McTigue, M. A., Williams, D. R., and Tainer, J. A. (1995) *J. Mol. Biol. 246*, 21−27.
36. Kraulis, P. J. (1991) *J. Appl. Crystallogr. 24*, 946−950.

BI990668U